Modeling of concrete behavior under high strain rates with inertially retarded damage

U. Häussler-Combe, M. Kitzig

Accepted Manuscript

Title: Modeling of concrete behavior under high strain rates with inertially retarded damage

Authors: U. Häußler-Combe, M. Kitzig

PII: S0734-743X(09)00040-2
DOI: 10.1016/j.ijimpeng.2009.02.004
Reference: IE 1753

To appear in: *International Journal of Impact Engineering*

Received Date: 24 September 2008
Revised Date: 3 February 2009
Accepted Date: 7 February 2009

Please cite this article as: Häußler-Combe U, Kitzig M. Modeling of concrete behavior under high strain rates with inertially retarded damage, International Journal of Impact Engineering (2009), doi: 10.1016/j.ijimpeng.2009.02.004

Modeling of concrete behavior under high strain rates with inertially retarded damage

U. Häußler-Combe*, M. Kitzig

Institute of Concrete Structures, Technische Universität Dresden, 01069 Dresden, Germany

Abstract

The paper proposes a novel approach to model the influence of high strain rates on the behavior of quasi-brittle materials like concrete. It is based on gradient continuum damage, where the gradient part is extended with an inertia of damage. This causes a retardation of damage due to the fact that micro-cracks cannot spread out arbitrarily fast. The application is demonstrated with uniaxial tensile wave propagation and for a plane stress case. Increasing strain rates lead to an expansion of the linear stress-strain behavior with stresses exceeding the quasistatic material strength.

Key words: Concrete; Strain rate influence; Retarded damage; Gradient damage

1 Introduction

The increase of concrete strength under high strain rates is important for extraordinary design situations, e.g., impact of vehicles and airplanes or blast waves from

* Corresponding author. Tel.: +49-351-463-39586; fax: +49-351-463-37279

Email-address: Ulrich.Haeussler-Combe@tu-dresden.de

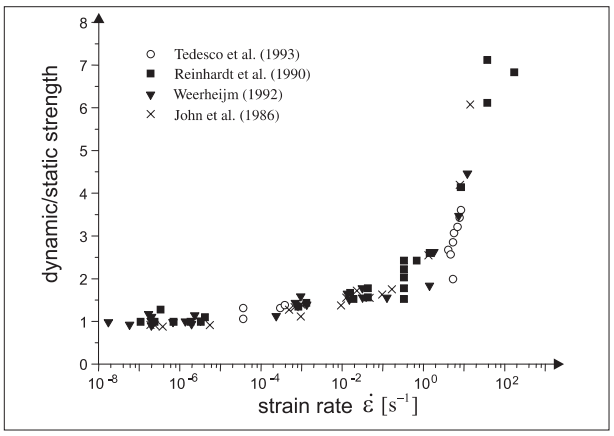

Fig. 1. Concrete tensile strength increase [3]

explosions or contact detonations upon concrete structures like bridges, offshore structures, tanks, chemical factories, power plants. A number of experimental investigations have been performed to study this effect, which can be observed for the compressive strength [1], and more pronounced for the tensile strength [2], see Fig. 1. Even in experiments it may become difficult to distinguish material behavior from structural system behavior, especially in the high dynamic range. Thus, inertial lateral confinement has been argued as a reason for strength increase. But this particular influence seems to play a role only for extremely high strain rates larger than 200 s^{-1} [4].

Generally, experiments should measure material properties and the influence of the experimental setup should be minimized as far as possible. Due to its heterogeneous structure this requirement is difficult to fulfill for concrete. A widely accepted experimental method is given with the Split-Hopkinson-bar [5], which up to now seems to be the most reliable measurement technique for material behavior under strain rates up to a range of $10^3\,\mathrm{s}^{-1}$ [6]. Extensive SHB investigations for concrete were performed, e.g., by [7–13]. Reliable results from experimental investigations are the basis for constitutive laws. A wide range of models have been proposed for concrete, which can be classified as microscopic, mesoscopic and macroscopic in a

first approach. While microscopic and mesoscopic models distinguish the concrete constituents in different orders of resolution, macroscopic models assume a homogeneous material. This allows the application of the methods of classical continuum mechanics and makes macroscopic models suitable for calculations of whole structures. The macroscopic approach will be used in the following. Constitutive laws for high strain rates are generally formulated as extensions of laws for the quasistatic case. Following basic concepts have been proposed:

- Quasistatic failure surfaces are enlarged depending on the strain rate [14,15]. The enlargement factor is calibrated according to results of experimental investigations. This proposal is empirical and does not include a physical background.
- Elastoplastic stress-strain relations are extended with rate dependent viscous parts, see, for instance [16,17], which temporarily leads to stresses beyond quasistatic failure conditions. This can physically be motivated by the resistance of a rapid movement of fluid phases within the microstructure of concrete. Beneath describing strain rate influence, this approach also leads to a problem regularization in the softening range of the material behavior.
- Consideration of the damage rate in damage evolution laws [18]. This leads to a delay effect for damage. The influence of this approach on strains and stresses has not been investigated in detail up to now.

All these approaches are directly coupled to rates of strains or stresses, i.e. a potential dynamic stress increase vanishes in the instant of strain or stress maximum values. This particular model behavior seems not to be fully reasonable. An alternative bases on the assumption that the activation of damage is retarded by inertial effects arising with micro-cracking. [19] implement this basic approach with a local dynamic relaxation for damage, which is derived from rheological models includ-

ing micro-mass elements. This decouples stresses from strain rates to some extent and leads to increasing dynamic stresses also for vanishing strain rates, but some complexity arises with the selection of the relaxation function and its parameters. The basic concept is also used in this paper, but will be simplified to a large extent. The formulation uses isotropic strain-based damage combined with a gradient part to include nonlocal damage. This serves for two purposes, (1) a problem regularization can be achieved and the hyperbolicity of the dynamic problem is preserved [20], and (2) the tight relation between damage and strain is resolved, which is used to assign damage with some type of inertia as a novel approach. This inertial part retards damage under high strain rates and temporarily leads to higher stresses compared to the quasistatic case.

In Section 2, a triaxial isotropic damage law is defined with a strain-based formulation. Regarding regularization, this law is extended with nonlocal damage in Section 3. This is performed with gradient continuum damage, and additionally extended with a damage inertia part. Thus, nonlocal damage is introduced as a variable on the system level leading to a specific dynamic finite element formulation, which is described in Section 4. The properties of gradient damage are discussed for the uniaxial tension bar under quasistatic loading in Section 5. Altogether, the basis is prepared for the investigation of wave propagation problems. This is at first performed for the uniaxial tension bar in Section 6, with load histories corresponding to constant strain rates in a range of $0.5 - 50\,\mathrm{s}^{-1}$. Especially the influence of the damage inertia parameter will be discussed. A two-dimensional application problem is demonstrated in Section 7. The paper is concluded in Section 8 by pointing out the potential for applications and further developments.

2 A constitutive law for concrete based on damage

A constitutive law based on isotropic damage

$$\boldsymbol{\sigma} = (1 - D)\, \mathbf{E} \cdot \boldsymbol{\epsilon} \tag{1}$$

is chosen for the following, with a scalar damage measure D, the stress vector $\boldsymbol{\sigma}$, the strain vector $\boldsymbol{\epsilon}$ and the elasticity matrix

$$\mathbf{E} = \frac{E(1-\nu)}{(1+\nu)(1-2\nu)} \begin{bmatrix} 1 & \frac{\nu}{1-\nu} & \frac{\nu}{1-\nu} & 0 & 0 & 0 \\ \frac{\nu}{1-\nu} & 1 & \frac{\nu}{1-\nu} & 0 & 0 & 0 \\ \frac{\nu}{1-\nu} & \frac{\nu}{1-\nu} & 1 & 0 & 0 & 0 \\ 0 & 0 & 0 & \frac{1-2\nu}{2(1-\nu)} & 0 & 0 \\ 0 & 0 & 0 & 0 & \frac{1-2\nu}{2(1-\nu)} & 0 \\ 0 & 0 & 0 & 0 & 0 & \frac{1-2\nu}{2(1-\nu)} \end{bmatrix}, \tag{2}$$

with Young's modulus E and Poisson's ratio ν. The values $E,\ \nu$ are constant, while the damage D depends on the loading history and has a range $0 \leq D \leq 1$. A widely accepted approach for damage evolution of quasi-brittle materials like concrete is based on a Weibull distribution of micro defects [21]. This leads to a form

$$D(\kappa) = \begin{cases} 0 & \kappa < e_0 \\ 1 - \mathrm{e}^{-\left(\frac{\kappa - e_0}{e_d}\right)^{g_d}} & \kappa \geq e_0 \end{cases} \tag{3}$$

introducing an equivalent damage strain κ, which is variable, and three material constants $e_d,\ e_0,\ g_d$. It is assumed that the equivalent damage strain κ amounts to

the longitudinal elastic strain in uniaxial compression. So, in uniaxial compression with monotonically increasing absolute values of strains, Eq. (1) reduces to

$$\sigma = \begin{cases} E\,\epsilon & |\epsilon| < e_0 \\ \mathrm{e}^{-\left(\frac{|\epsilon|-e_0}{e_d}\right)^{g_d}} E\,\epsilon & |\epsilon| \geq e_0 \end{cases} \tag{4}$$

with the longitudinal stress σ and the longitudinal strain ϵ. From this relation the material parameters e_d, e_0, g_d can be derived from well-known stress-strain relations for uniaxial compression, see e.g. [14]. Corresponding values of the material parameters are given in Table 1 for typical concrete grades.

Multiaxial loading states can be described by a relation combining the equivalent damage strain κ with the multiaxial strain state $\boldsymbol{\epsilon}$. Here a strength failure condition is chosen according to [22], which is transformed from stress space into strain space and finally generalized into a damage function F [23]

$$F(\boldsymbol{\epsilon}, \kappa) = a_1\, J_\epsilon + \kappa \left[a_2 \sqrt{J_\epsilon} + a_3\, \epsilon_1 + a_4\, I_\epsilon \right] - \kappa^2 = 0 \tag{5}$$

with the second invariant J_ϵ of the strain deviator, the first invariant I_ϵ of the strain tensor, the largest (signed) principal strain ϵ_1 and four material constants $a_1 \ldots a_4$. The parameters $a_1 \ldots a_4$ are obtained considering uniaxial and multiaxial special cases, which ensures the above-mentioned equivalence of the damage strain and the longitudinal elastic strain in uniaxial compression. Finally, the formalism is completed with Kuhn-Tucker conditions

$$F \leq 0, \quad \dot{D} \geq 0, \quad \dot{D}\, F = 0 \tag{6}$$

with the rate $\dot{D}$ of damage. Values $\dot{D} > 0,\ F = 0,\ \dot{F} = 0$ indicate loading with increasing damage, while $\dot{D} = 0,\ F \leq 0$ indicate all other states with constant

damage. In case of loading the consistency condition $\dot{F} = 0$ leads to

$$\mathbf{n}^T \cdot \dot{\boldsymbol{\epsilon}} - H\,\dot{\kappa} = 0 \tag{7}$$

with

$$\begin{aligned} \mathbf{n} &= \frac{\partial F}{\partial \boldsymbol{\epsilon}} = \left(a_1 + a_2\,\frac{\kappa}{2\sqrt{J_\epsilon}}\right)\boldsymbol{\epsilon}^{dev} + \kappa\,(a_3\ \ \mathbf{d}_1 \otimes \mathbf{d}_1 + a_4\,\mathbf{I}) \\ H &= -\frac{\partial F}{\partial \kappa} = a_2\,\sqrt{J_\epsilon} + a_3\,\epsilon_1 + a_4\,I_\epsilon - 2\kappa \end{aligned} \tag{8}$$

with the direction $\mathbf{d}_1$ of the largest principal strain ϵ_1, the dyadic product $\otimes$, and the 2nd order unit tensor $\mathbf{I}$. The four material constants $a_1 \ldots a_4$ describe the shape of a damage surface in the principal strain space, which can be transformed into a surface in the principal stress space with Eq. (1). Increasing damage and the expansion of the damage surface is ruled by increasing values κ, see Eqns. (3), (5). The equivalent damage strain κ has a distinct value κ_1, which marks the strength of the material. Strength corresponds to maximum stress values, e.g. the uniaxial compressive strength f_c under uniaxial loading with a longitudinal strain ϵ_{c1} and $\kappa_1 = |\epsilon_{c1}|$ by definition. Values $\dot{\kappa} > 0,\ \kappa < \kappa_1$ indicate the hardening range with expanding surfaces of damage and the corresponding principal stress, while $\dot{\kappa} > 0,\ \kappa > \kappa_1$ indicate the softening range with expanding surfaces of damage and contracting surfaces of the corresponding principal stress. The intermediate state $\kappa = \kappa_1$ gives the strength or failure state, respectively. Certain strength states, like the uniaxial compressive strength, the uniaxial tensile strength, the biaxial strength and the triaxial strength with a given confining pressure, can be used to determine the values of the parameters $a_1 \ldots a_4$ in Eq. (5). The values for the chosen concrete grades are given in Table 1.

Basically, the formulation is fully three-dimensional. In this paper the uniaxial tensile case will be investigated in the context of uniaxial stress propagation under high strain rates. Let ϵ_1 be the longitudinal strain. So lateral strains are given by $\epsilon_2 = \epsilon_3 = -\nu\,\epsilon_1$ with Eq. (1). Hence, the damage function Eq. (5) leads to

$$F = a_1 \frac{(1+\nu)^2\,\epsilon_1^2}{3} + \kappa \left(a_2 \frac{1+\nu}{\sqrt{3}} + a_3 + a_4\,(1-2\nu) \right) \epsilon_1 - \kappa^2 \tag{9}$$

With $F = 0$, this can be solved for the positive value of κ to give the equivalent damage strain for uniaxial tension depending on the monotonically increasing longitudinal tensile strain

$$\kappa = b\,\epsilon_1 \tag{10}$$

with a constant value b, which can be derived from the constant material parameters ν, $a_1 \ldots a_4$. Thus, in analogy to Eq. (4) the stress-strain relation for the uniaxial tension case with monotonic loading is given by

$$\sigma = \begin{cases} E\,\epsilon_1 & \epsilon_1 < e_0/b \\ \mathrm{e}^{-\left(\frac{b\,\epsilon_1 - e_0}{e_d}\right)^{g_d}} E\,\epsilon_1 & \epsilon_1 \geq e_0/b \end{cases} \tag{11}$$

Computed stress-strain curves for tension are shown in Fig. 2. It can be seen that the tensile behavior is characterized by a limited tensile strength followed by a softening branch. From a phenomenological point of view softening is connected with localization, i.e. narrow bands with very high strains, which leads to a fundamental mesh sensitivity of numerical calculations [24]. A number of concepts have been proposed to resolve localization zones and to reach mesh objective results or a regularization, respectively. From these concepts gradient continuum damage will be used in the following.

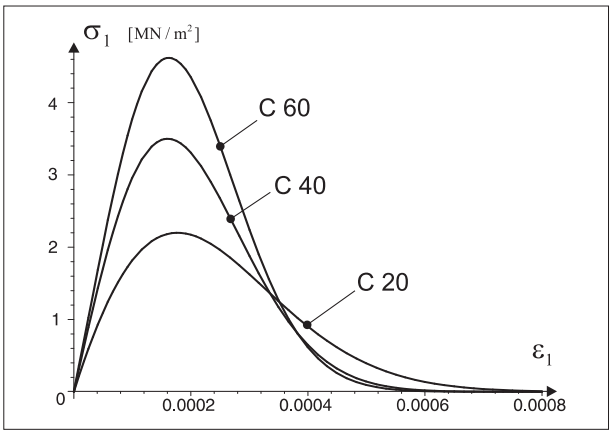

Fig. 2. Uniaxial quasistatic tensile stress-strain relations

3 Gradient based damage extended with inertia

Under ongoing loading concrete shows a quasi-brittle behavior due to its heterogeneous structure, i.e. a development of micro-cracks evolving into macro-cracks within a so-called process zone. The final formation of macro-cracks consumes a considerable amount of energy, which leads to a size effect and may contribute to a ductile behavior of whole structures. The size of the process zone or the measure of crack energy corresponds to the extent of the material heterogeneity. Regarding concrete, heterogeneity in the mesoscopic scale is a matter of aggregates binded by a cement matrix. This leads to a non-locality of actions in the homogenized macroscopic scale, where in case of damage a given spatial coordinate $\mathbf{x}$ is assigned a nonlocal value $\bar{\kappa}$ of the equivalent damage strain κ in a neighborhood of $\mathbf{x}$

$$\bar{\kappa}(\mathbf{x}) = \frac{1}{S}\int g(\mathbf{s})\,\kappa(\mathbf{x}+\mathbf{s})\,\mathrm{d}V \tag{12}$$

with the variable spatial coordinate $\mathbf{s}$ and a weighting function

$$g(\mathbf{s}) = \mathrm{e}^{-\frac{\mathbf{s}^2}{2\mathrm{R}^2}}, \qquad S = \int g(\mathbf{s})\,\mathrm{d}V. \tag{13}$$

Generally, the weighting function g is bell-shaped, for alternative forms see [25]. The interaction range R determines the decay of weighting for a given value $\mathbf{s}$, large values lead to a large range of the weighting function, small values to a small range. R introduces a length scale in the material model, which is assumed as a material constant. Its determination will be discussed in Section 5.

The approach Eq. (12) reduces local extreme values of κ while broadening their base. In contrast, constant values κ lead to the same values $\bar{\kappa}$. The integral form Eq. (12) can be transformed into a differential regularization equation

$$\bar{\kappa}(\mathbf{x}) - c\,\Delta\bar{\kappa}(\mathbf{x}) = \kappa(\mathbf{x}), \qquad c = \frac{R^2}{2} \tag{14}$$

with the Laplace operator Δ, where higher order terms have been neglected [26]. This partial differential equation of second order in the nonlocal equivalent damage strain $\bar{\kappa}$ forms the base of gradient continuum damage [27]. Let us assume a given strain field so that Eq. (5) provides a field $\kappa(\mathbf{x})$ for the local equivalent damage strain. Then Eq. (14) serves to determine the nonlocal field $\bar{\kappa}(\mathbf{x})$. These nonlocal values are used for the constitutive law instead of the local values, as κ is replaced by $\bar{\kappa}$ in Eq. (3). This approach enforces a finite width of the localization zone independent of meshing, where larger values of the interaction range R lead to an increasing localization zone width.

Up to now, gradient continuum damage has been discussed with respect to regularization, where Eq. (14) introduces the nonlocal equivalent damage strain $\bar{\kappa}$ as a further basic unknown beneath the field of displacements $\mathbf{u}$. All other variable parameters can be derived from $\bar{\kappa}$, $\mathbf{u}$, but these two remain in a set of differential equations or their weak counterparts. Now we assume that a rapid change of damage is joined with inertial effects like the rapid change of displacements with a

mass inertia. In other words, the material stiffness or compliance, respectively, will be influenced by an increment of the damage measure only after a certain delay of time. This is based on the idea, that micro-cracks cannot spread out arbitrarily fast as a movement of internal crack faces is involved, i.e. a movement of masses on a microscopic scale. Hence one can conclude that inertia effects in concrete on microlevel mainly determine its strain rate dependent phenomenological properties on macrolevel [19]. Thus, Eq. (14) is extended by

$$m_\kappa \, \ddot{\bar{\kappa}}(\mathbf{x}) + \bar{\kappa}(\mathbf{x}) - c \, \Delta \bar{\kappa}(\mathbf{x}) = \kappa(\mathbf{x}) \tag{15}$$

with the acceleration $\ddot{\bar{\kappa}}$ of $\bar{\kappa}$ and a novel damage inertia m_κ. With the formulation of Eq. (15), the proposed damage approach may be regarded as nonlocal in time and place [28]. This will be demonstrated in Sections 5 and 6. The parameter m_κ is assumed to be a material constant. A major item of this paper is to investigate the influence of this parameter on the material behavior under high strain rates. For uniaxial wave propagation this will be performed in a parametric study in Section 6.

4 Discretization

The dynamically extended gradient damage approach shall be incorporated in the finite element method. To begin with, Eq. (15) has to be transformed into a weak form. The standard way starts with

$$\begin{aligned} &\int_V \delta\bar{\kappa} \left[\kappa - m_\kappa \ddot{\bar{\kappa}} - \bar{\kappa} + c \, \Delta \bar{\kappa} \right] \mathrm{d}V = \\ &\int_V \delta\bar{\kappa} \, \kappa \, \mathrm{d}V - \int_V m_\kappa \, \delta\bar{\kappa} \, \ddot{\bar{\kappa}} \, \mathrm{d}V - \int_V \delta\bar{\kappa} \, \bar{\kappa} \, \mathrm{d}V + \int_V c \, \delta\bar{\kappa} \, \Delta\bar{\kappa} \, \mathrm{d}V = 0 \end{aligned} \tag{16}$$

with a test function $\delta\bar{\kappa}$. The product rule of differentiation leads to

$$\delta\bar{\kappa}\,\Delta\bar{\kappa} = \operatorname{div}\left(\delta\bar{\kappa}\,\nabla\bar{\kappa}\right) - \nabla\delta\bar{\kappa}\cdot\nabla\bar{\kappa} \tag{17}$$

with the scalar product $\cdot$, the divergence operator div and the nabla operator ∇. Using the Gauss theorem we have

$$\int_V \operatorname{div}\left(\delta\bar{\kappa}\,\nabla\bar{\kappa}\right)\,\mathrm{d}V = \int_A \delta\bar{\kappa}\,\mathbf{n}\cdot\nabla\bar{\kappa}\,\mathrm{d}A \tag{18}$$

with the outer surface normal $\mathbf{n}$. Thus, Eq. (16) can be written in a form

$$\begin{aligned}\int_V m_\kappa\,\delta\bar{\kappa}\,\ddot{\bar{\kappa}}\,\mathrm{d}V + \int_V \delta\bar{\kappa}\,\bar{\kappa}\,\mathrm{d}V + \int_V c\,\nabla\delta\bar{\kappa}\cdot\nabla\bar{\kappa}\,\mathrm{d}V \\ = \int_V \delta\bar{\kappa}\,\kappa\,\mathrm{d}V + \int_A c\,\delta\bar{\kappa}\,\mathbf{n}\cdot\nabla\bar{\kappa}\,\mathrm{d}A\end{aligned} \tag{19}$$

This form is suited for a discretization with respect to the nonlocal equivalent damage strain $\bar{\kappa}$ while the local value κ is given. The surface integral part remains to be discussed. Additional boundary conditions for the nonlocal equivalent damage strain are required, i.e. either $\bar{\kappa}$ or the normal derivative $\mathbf{n}\cdot\nabla\bar{\kappa}$ have to be specified in every point of the surface A. Let us assume, that $\bar{\kappa}$ can be prescribed along a part A_κ of the whole surface A and that $\delta\bar{\kappa} = 0$ can be set along A_κ. Furthermore, we consider cases with strains localizing in narrow bands with orientations that near the surface are approximately perpendicular to the boundary with the normal $\mathbf{n}$. As any major damage gradients $\nabla\bar{\kappa}$ arise perpendicularly to the band of localization, the condition $\mathbf{n}\cdot\nabla\bar{\kappa} = 0$ can be set along the remaining part of A where $\bar{\kappa}$ is not prescribed [26]. Finally, Eq. (19) is simplified with

$$\int_V m_\kappa\,\delta\bar{\kappa}\,\ddot{\bar{\kappa}}\,\mathrm{d}V + \int_V \delta\bar{\kappa}\,\bar{\kappa}\,\mathrm{d}V + \int_V c\,\nabla\delta\bar{\kappa}\cdot\nabla\bar{\kappa}\,\mathrm{d}V = \int_V \delta\bar{\kappa}\,\kappa\,\mathrm{d}V \tag{20}$$

which will be used in the following and has to be combined with the constitutive law. First of all, the local κ in Eq. (3) is replaced by the nonlocal $\bar{\kappa}$

$$D(\bar{\kappa}) = 1 - \mathrm{e}^{-\left(\frac{\bar{\kappa}-e_0}{e_d}\right)^{g_d}}, \qquad \bar{\kappa} \geq e_0 \tag{21}$$

and we obtain the increment of damage $\mathrm{d}D$ depending on the increment $\mathrm{d}\bar{\kappa}$ of the nonlocal equivalent damage

$$\mathrm{d}D = \frac{\mathrm{d}D}{\mathrm{d}\bar{\kappa}}\,\mathrm{d}\bar{\kappa} = \frac{1}{h}\,\mathrm{d}\bar{\kappa}, \qquad \frac{1}{h} = \frac{g_d\left(\frac{\bar{\kappa}-e_0}{e_d}\right)^{g_d}}{\bar{\kappa}-e_0}\ \mathrm{e}^{-\left(\frac{\bar{\kappa}-e_0}{e_d}\right)^{g_d}} \tag{22}$$

With Eq. (1), the stress increment is given by

$$\begin{aligned} \mathrm{d}\boldsymbol{\sigma} &= (1-D)\,\mathbf{E}\cdot\mathrm{d}\boldsymbol{\epsilon} - \mathrm{d}D\,\mathbf{E}\cdot\boldsymbol{\epsilon} = (1-D)\,\mathbf{E}\cdot\mathrm{d}\boldsymbol{\epsilon} - \frac{\mathrm{d}\bar{\kappa}}{h}\ \boldsymbol{\sigma}_{el} \\ \boldsymbol{\sigma}_{el} &= \mathbf{E}\cdot\boldsymbol{\epsilon} \end{aligned} \tag{23}$$

This completes the material and gradient damage parts. Equilibrium of forces has the condition

$$\int_V \delta\mathbf{u}\cdot\ddot{\mathbf{u}}\,\rho\mathrm{d}V + \int_V \delta\boldsymbol{\epsilon}\cdot\boldsymbol{\sigma}\,\mathrm{d}V = \int_V \delta\mathbf{u}\cdot\mathbf{b}\,\mathrm{d}V + \int_{A_t} \delta\mathbf{u}\cdot\mathbf{t}\,\mathrm{d}A \tag{24}$$

with the acceleration $\ddot{\mathbf{u}}$, the specific mass ρ, body forces $\mathbf{b}$ and surface tractions $\mathbf{t}$. Both weak forms Eqns. (20,24) are discretized by

$$\mathbf{u} = \mathbf{N}_u\cdot\mathbf{u}_I, \quad \bar{\kappa} = \mathbf{N}_\kappa\cdot\bar{\boldsymbol{\kappa}}_I \tag{25}$$

with the matrices $\mathbf{N}_u,\ \mathbf{N}_\kappa$ of form functions and the vectors $\mathbf{u}_I,\ \bar{\boldsymbol{\kappa}}_I$ of nodal values of displacement and nonlocal equivalent damage strain. The spatial derivatives and their increments are given by

$$\boldsymbol{\epsilon} = \mathbf{B}_u\cdot\mathbf{u}_I, \quad \mathrm{d}\boldsymbol{\epsilon} = \mathbf{B}_u\cdot\mathrm{d}\mathbf{u}_I, \quad \nabla\bar{\kappa} = \mathbf{B}_\kappa\cdot\bar{\boldsymbol{\kappa}}_I, \quad \mathrm{d}\,\nabla\bar{\kappa} = \mathbf{B}_\kappa\cdot\mathrm{d}\bar{\boldsymbol{\kappa}}_I \tag{26}$$

The test functions $\delta\mathbf{u}$, $\delta\bar{\kappa}$ are discretized in the same way. Using Eqns. (25,26) together with the weak forms Eqns. (20,24) leads to

$$\mathbf{M}\cdot\ddot{\mathbf{a}} = \mathbf{f} - \mathbf{r} \tag{27}$$

with

$$\mathbf{a} = \begin{pmatrix} \mathbf{u}_I \\ \\ \bar{\boldsymbol{\kappa}}_I \end{pmatrix} \tag{28}$$

with the nodal nonlocal equivalent damage strains as global unknowns beneath the nodal displacements and

$$\mathbf{M} = \begin{bmatrix} \mathbf{M}_u & 0 \\ \\ 0 & \mathbf{M}_\kappa \end{bmatrix}, \quad \mathbf{r} = \begin{pmatrix} \mathbf{r}_u \\ \\ \mathbf{r}_\kappa \end{pmatrix}, \quad \mathbf{f} = \begin{pmatrix} \mathbf{f}_u \\ \\ \mathbf{f}_\kappa \end{pmatrix} \tag{29}$$

and

$$\begin{aligned} \mathbf{M}_u &= \int_V \mathbf{N}_u^T\cdot\mathbf{N}_u\,\rho\mathrm{d}V, & \mathbf{M}_\kappa &= \int_V \mathbf{N}_\kappa^T\cdot\mathbf{N}_\kappa\,m_\kappa\mathrm{d}V \\ \mathbf{r}_u &= \int_V \mathbf{B}_u^T\cdot\boldsymbol{\sigma}\,\mathrm{d}V, & \mathbf{r}_\kappa &= \int_V \left(\mathbf{N}_\kappa^T\bar{\kappa} + \mathbf{B}_\kappa^T\cdot\nabla\bar{\kappa}\,c\right)\mathrm{d}V \\ \mathbf{f}_u &= \int_V \mathbf{N}_u^T\cdot\mathbf{b}\,\mathrm{d}V + \int_{A_t} \mathbf{N}_u^T\cdot\mathbf{t}\,\mathrm{d}A, & \mathbf{f}_\kappa &= \int_V \mathbf{N}_\kappa^T\,\kappa\,\mathrm{d}V \end{aligned} \tag{30}$$

Eq. (27) forms a system of nonlinear ordinary differential equations of 2nd order in time t. The u-part and the κ-part are coupled by the damage D in the stress $\boldsymbol{\sigma}$, see Eqns. (1,21), and by the local equivalent damage strain κ in the damage function F, see Eq. (5). Explicit or implicit time integration schemes can be used to determine

$\mathbf{a}$ during time. Implicit schemes require a tangent stiffness matrix

$$\mathbf{K} = -\left(\frac{\partial \mathbf{f}}{\partial \mathbf{a}} - \frac{\partial \mathbf{r}}{\partial \mathbf{a}}\right) = \begin{bmatrix} \frac{\partial \mathbf{r}_u}{\partial \mathbf{u}_I} & \frac{\partial \mathbf{r}_u}{\partial \boldsymbol{\kappa}_I} \\ -\frac{\partial \mathbf{f}_\kappa}{\partial \mathbf{u}_I} & \frac{\partial \mathbf{r}_\kappa}{\partial \boldsymbol{\kappa}_I} \end{bmatrix} = \begin{bmatrix} \mathbf{K}_{uu} & \mathbf{K}_{u\kappa} \\ \mathbf{K}_{\kappa u} & \mathbf{K}_{\kappa\kappa} \end{bmatrix} \tag{31}$$

From Eqns. $(30)_3$, (23) and $\mathrm{d}\kappa = \mathbf{n}^T \cdot \mathrm{d}\boldsymbol{\epsilon}/H$, see Eq. (7), we have

$$\begin{aligned} \mathbf{K}_{uu} &= \int_V (1-D)\, \mathbf{B}_u^T \cdot \mathbf{E} \cdot \mathbf{B}_u \, \mathrm{d}V \\ \mathbf{K}_{u\kappa} &= -\int_V \frac{1}{h}\, \mathbf{B}_u^T \cdot \boldsymbol{\sigma}_{el} \cdot \mathbf{N}_\kappa \, \mathrm{d}V \\ \mathbf{K}_{\kappa u} &= -\int_V \frac{1}{H}\, \mathbf{N}_\kappa^T \cdot \mathbf{n}^T \cdot \mathbf{B}_u \, \mathrm{d}V \\ \mathbf{K}_{\kappa\kappa} &= \int_V \left(\mathbf{N}_\kappa^T \cdot \mathbf{N}_\kappa + \mathbf{B}_\kappa^T \cdot \mathbf{B}_\kappa \, c\right) \mathrm{d}V \end{aligned} \tag{32}$$

for the loading case, while $\mathbf{K}_{u\kappa} = 0$ for unloading. It can be seen that $\mathbf{K}$ is unsymmetric, but this generally occurs for damage formulations not derived from potentials with the principle of maximum dissipation.

5 The uniaxial tension bar under quasistatic loading

It remains to determine the value of the interaction range R. We consider that localization ends up in macro cracking and dissipation of crack energy. With a continuum approach crack energy for uniaxial tension results from

$$G_f = \int_0^{d_w} g(\epsilon)\, \mathrm{d}w \tag{33}$$

with the localization zone width d_w, its variable w and a specific crack energy

$$g(\epsilon) = \int_{\epsilon_{ct}}^{\epsilon} \sigma(\epsilon')\,\mathrm{d}\epsilon', \qquad \epsilon \geq \epsilon_{ct} \tag{34}$$

where the integration starts from concrete tensile strength with a strain ϵ_{ct} and $\sigma(\epsilon)$ is given by Eq. (11). The crack energy G_f is assumed to be a material property. Its value is, within a certain range, independent from the other material parameters. Typical values are given in Table 1. In contrast, the specific crack energy g results from integration of the decreasing branch of the stress-strain curve, see Fig. 2, and fully depends on the other material parameters.

Obviously there should be a relation between the interaction range R and the localization zone width d_w. This relation can be determined with an inverse analysis by a parameter study performed on a uniaxial tension bar under quasistatic loading. The tension bar system is shown in Fig. 3, where the length is chosen with $L = 0.5\,\mathrm{m}$. The displacement is fixed at the left side, while the right side displacement is prescribed. A concrete grade C 40 according to Table 1 is used as material. Damage boundary conditions are prescribed with $\bar{\kappa} = 0$ for both end nodes, which may be regarded as a model for a bar with a sligthly higher strength at the lateral

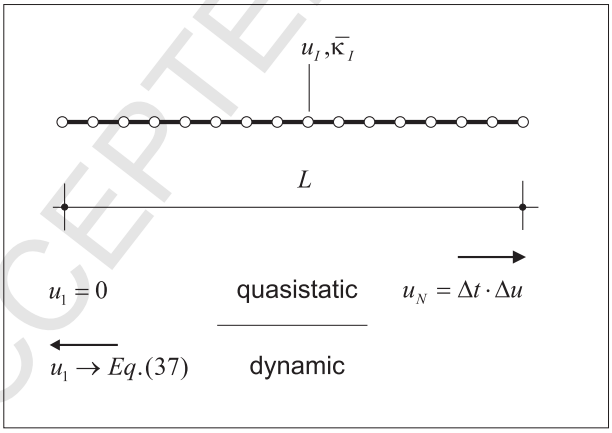

Fig. 3. Tension bar system

parts. This leads to a failure in exactly one point in the central part even in case of a homogeneous stress. A number of 500 uniaxial bar elements with two nodes and a linear approach is chosen, both for $\mathbf{u}$ and $\bar{\boldsymbol{\kappa}}$. Finer discretizations do not lead to a significant change of results. As the quasistatic behavior is examined, the inertial part $\mathbf{M}$ is neglected in Eq. (27). The prescribed right side displacement is incrementally applied with an arc length control, while an equilibrium iteration is performed with the Newton-Raphson method within each load increment. A computed load displacement curve is shown in Fig. 4, where a value $R = 0.03\,\mathrm{m}$ is chosen. As a typical characteristic of softening materials a snap-back behavior oc-

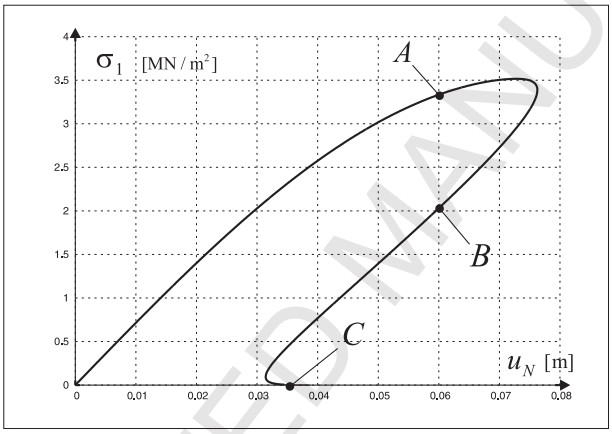

Fig. 4. Load-displacement curve of tension bar under quasistatic loading

curs, but due to the regularization this is independent from the discretization and mesh objectivity is preserved. The strain distribution along the bar for two stages of the load displacement curve, stage A before and stage B after the peak load, is shown in Fig. 5. While strain is nearly constant in stage A, a localization zone with a very high strain develops in stage B. The crack energy is determined for the final stage C of the load-displacement curve, when the localized section reaches a strain with zero stress on the softening branch of the stress-strain curve, see Fig. (2). The localization zone width is determined with the condition that its strains are larger than the strain ϵ_{ct} of the tensile strength f_{ct}. Moreover, the continuous variations

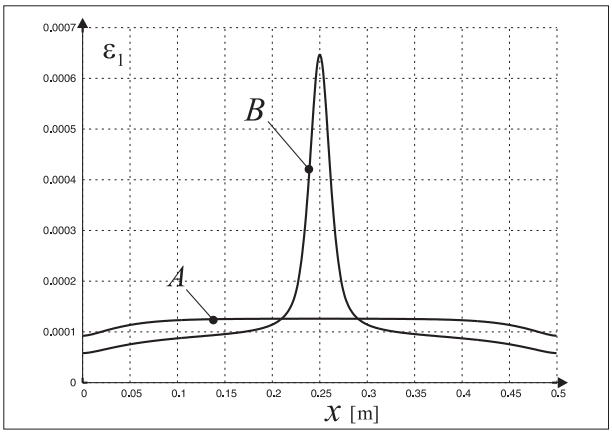

Fig. 5. Strain distributions along tension bar under quasistatic loading

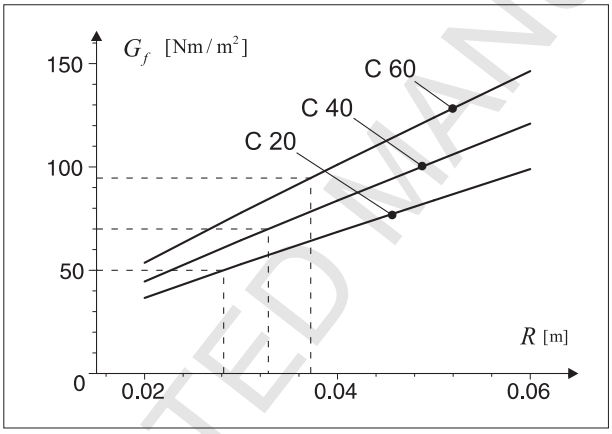

Fig. 6. Computed crack energy depending on interaction range R

of ϵ and of the specific crack energy $g(\epsilon)$ within the localization zone are regarded for the numerical integration of the crack energy G_f with Eq. (33). The computed value of G_f depending on the assumed value of R is shown in Fig. 6 for all concrete grades of Table 1. Approximately, a linear increase of the crack energy is given with increasing interaction range. It has to be pointed out that this particular relation depends on the course of the stress-strain curve in the softening range, see Fig. 2. A value $R = 0.03\,\mathrm{m}$ is chosen for the following investigations.

6 Application for uniaxial wave propagation

For the linear elastic case uniaxial wave propagation is described by

$$E \frac{\partial^2 u}{\partial x^2} = \varrho \frac{\partial^2 u}{\partial t^2} \tag{35}$$

with the displacement u, Young's modulus E and the specific mass ϱ. A bar is considered, which is loaded from its left side $x = 0$. A solution of Eq. (35) is then given by

$$u(x,t) = f(z), \quad z = \langle ct - x \rangle , \quad c = \sqrt{\frac{E}{\varrho}} \tag{36}$$

with an arbitrary function $f(z)$ and Mc-Auley brackets $\langle\rangle$: $\langle a \rangle = a$ if $a > 0$, $\langle a \rangle = 0$ otherwise. Eq. (36) describes a wave starting at the left side for $t = 0$ and moving to the right side with a speed c. A constant strain rate $\dot{\epsilon}_0$ is reached with a particular form

$$u(x,t) = -\frac{\dot{\epsilon}_0}{2c} \langle ct - x \rangle^2 \tag{37}$$

with a prescribed displacement on the left side

$$u(0,t) = -\frac{1}{2} \dot{\epsilon}_0 \, ct^2, \qquad t \geq 0 \tag{38}$$

leading to a tensile wave and a strain

$$\epsilon(x,t) = \frac{\dot{\epsilon}_0}{c} \langle ct - x \rangle , \qquad \dot{\epsilon}(x,t) = \dot{\epsilon}_0 \tag{39}$$

A concrete C 40 is chosen for a reference case, with $E = 36\,000\,\mathrm{MN/m^2}$, $\varrho = 2.4 \cdot 10^{-3}\,\mathrm{MN\,s^2/m^4}$. This leads to a wave speed $c = 3\,873\,\mathrm{m/s}$ for a linear elastic behavior and results in a stress wave propagation as shown in Fig. 7. With

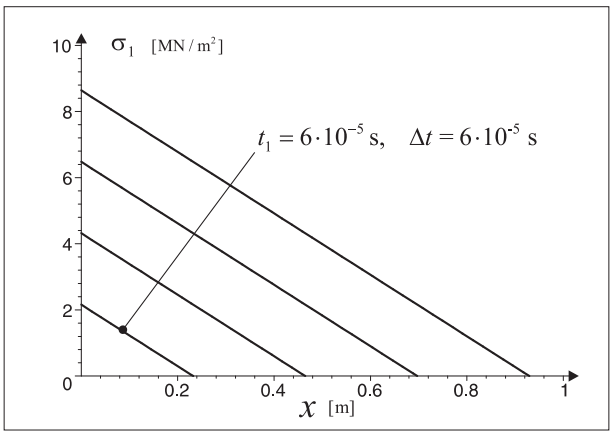

Fig. 7. Linear elastic wave propagation

$\dot{\epsilon}_0 = 1\,\mathrm{s}^{-1}$ a value of the concrete's quasistatic tensile strength $f_{ct} = 3.5\,\mathrm{MN/m}^2$ is reached after a time $t = 0.97 \cdot 10^{-4}\,\mathrm{s}$, and the stress wave has preceded to a point $x = 0.38\,\mathrm{m}$. Hence, for the following studies a bar length $L = 1.0\,\mathrm{m}$ is chosen, with a range of nominal strain rates $0.5\,\mathrm{s}^{-1} \leq \dot{\epsilon}_0 \leq 50\,\mathrm{s}^{-1}$. As the quasistatic tensile strength is by far exceeded within this parameter range, the nonlinear material behavior is regarded together with the gradient damage. Again, the discretization is chosen with 500 uniaxial bar elements with two nodes and a linear approach, and again finer discretizations do not lead to a significant change of results. As to the boundary conditions, the displacement of the left point of loading is prescribed according to Eq. (38). Damage boundary conditions are assumed with $\mathbf{n} \cdot \nabla\bar{\kappa} = \partial\bar{\kappa}/\partial x = 0$ on both sides. The implicit Newmark β-method with a Rayleigh damping $\mathbf{C} = \alpha_1\mathbf{M} + \alpha_2\mathbf{K}$ is used for time integration, with $\alpha_1 = 1 \cdot 10^{-6}$, $\alpha_2 = 5 \cdot 10^{-6}$ and a time step $\Delta t = 1 \cdot 10^{-6}\,\mathrm{s}$. This prevents high frequency oscillations of the computed velocities and strain rates, while the influence on absolute values of stress and strain remains below 1 % compared to the undamped case.

For the reference case the nominal strain rate is chosen with $\dot{\epsilon}_0 = 5\,\mathrm{s}^{-1}$ and the damage inertia, see Eq. (15), with $m_\kappa = 2 \cdot 10^{-9}\,\mathrm{s}^2$. The computed stress distribu-

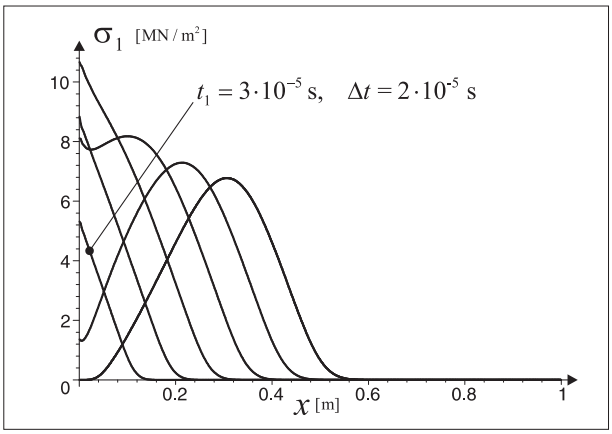

Fig. 8. Reference case: stresses along the bar

tions along the bar are shown in Fig. 8 for different time steps, with a beginning $t_1 = 3 \cdot 10^{-5}\,\mathrm{s}$ and an interval $\Delta t = 2 \cdot 10^{-5}\,\mathrm{s}$. This starts with an elastic behavior leading to stresses with a maximum value of $10.66\,\mathrm{MN/m^2}$, which is temporarily much higher than the quasistatic tensile strength of $3.5\,\mathrm{MN/m^2}$. Initiated from the loading point a decrease of stresses follows in later stages, while the displacement of the loading point is continuously determined by Eq. (38). In the following pe-

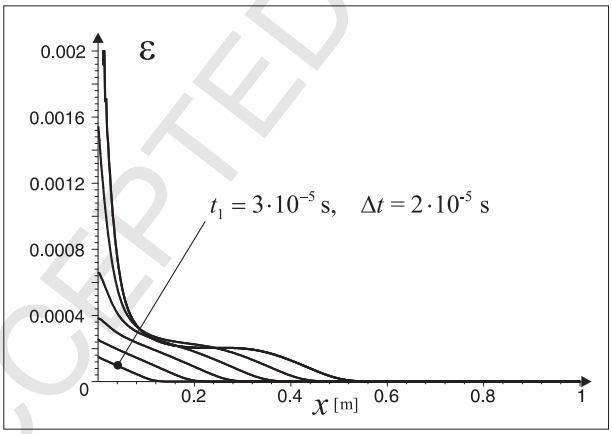

Fig. 9. Reference case: strains

riod the stress drops to zero in the left part while still propagating along the bar. Accompanying results for the same time steps with their distribution along the bar length are given for strains, Fig. 9, strain rates, Fig. 10, and damage, Fig. 11. In the early stages without major damage a linear behavior can be seen for strains with

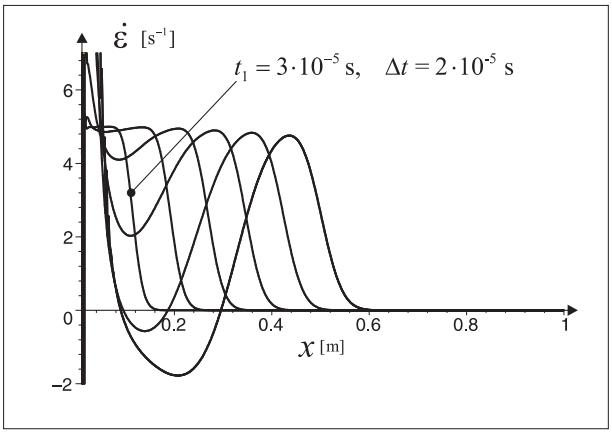

Fig. 10. Reference case: strain rates

356 constant strain rates. After exceeding the maximum stresses in later stages dam-
age rapidly grows. As the decrease of stresses corresponds to increasing strains in

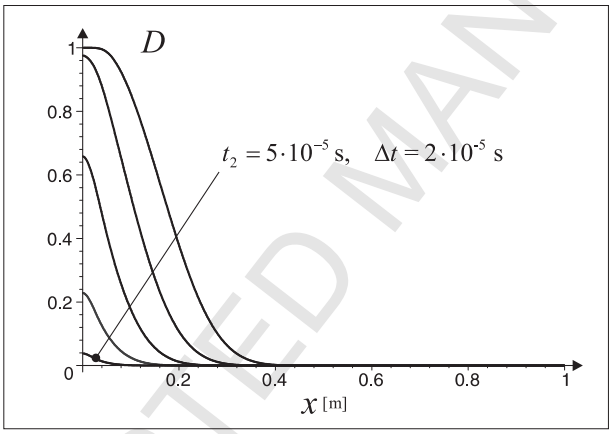

Fig. 11. Reference case: damage

357

358 the softening range, strains strongly grow in the loading point. Corresponding to
359 this behavior, the strain rates within the bar are not maintained in the softening
360 range. Finally, stress-strain relations can be determined for high strain rates. For
361 this purpose, the values of stresses and strains are evaluated for the particular place
362 in the bar, at which the strain rate nearly remains constant for each time step. This
363 place can be obtained from Fig. 10 and is assumed to exist for all prescribed dis-
364 placements according to Eq. (38). In the reference case, an approximately constant
365 strain rate $\dot{\epsilon} = 5\,\mathrm{s}^{-1}$ can be observed for $x \approx 0.05m$. In Fig. 12, the corresponding

stress-strain relation is contrasted with the curve obtained for quasistatic loading. Inertially retarded damage principally cannot change the material behavior in un-

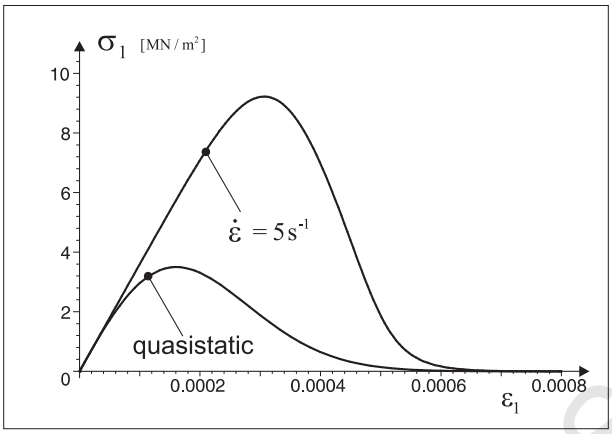

Fig. 12. Reference case: stress-strain relations

damaged states. Thus, both curves share the same initial course and have the same initial Young's modulus, irrespective of the strain rate. This behavior is confirmed by most experimental investigations [1]. Furthermore, it can be observed that a linear stress-strain behavior extends much farther compared to the quasistatic case, i.e. much higher stresses are reached with moderately higher strains.

Basically, the same results occur with the variation of both the nominal strain rate and the damage inertia. The maximum stress reached during the loading history is of particular interest. Fig. 13 shows the maximum stress values depending on the nominal strain rate $\dot{\epsilon}_0$ for several values of the damage inertia m_κ. Again a concrete grade C 40 is used, and the computed maximum stress values are related to the quasistatic tensile strength $f_{ct} = 3.5\,\mathrm{MN/m^2}$. Experimental data from Fig. 1 are also shown together with the computed curves. It can be seen, that the retarded damage model in principal agrees with the experimentally observed behavior. Computed strength increase seems to be underestimated for low nominal strain rates $\dot{\epsilon}_0 < 2\,\mathrm{s}^{-1}$. This indicates that movement of fluid phases and the viscosity have a larger influence in this range, which is not covered by the present approach and

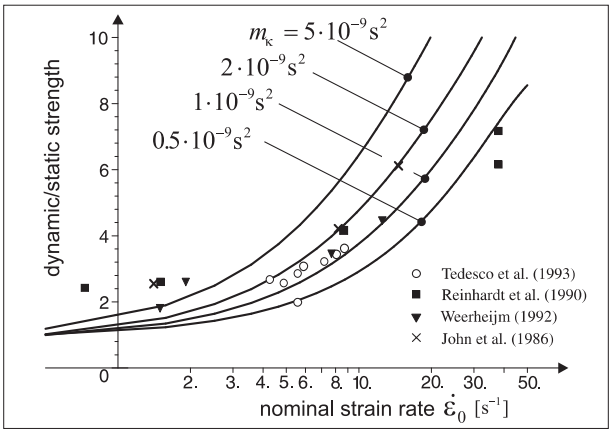

Fig. 13. Tensile strength C 40 depending on nominal strain rate and damage inertia

suggests a combination of both. Experimental data for larger nominal strain rates $\dot{\epsilon}_0 > 20\,\mathrm{s}^{-1}$ are rare. Furthermore, all investigations show that actual strain rates do not have constant values in real situations.

Up to now, the value of m_κ can only be estimated with an inverse analysis such that computed values fit to experimentally observed data. Following the previous parameter study, values near $2 \cdot 10^{-9}\,\mathrm{s}^2$ give the best agreement for a concrete grade C 40. This value is also chosen for further computations, which are performed for the concrete grades C 20 and C 60. This leads to similar results. Fig. 14 shows the

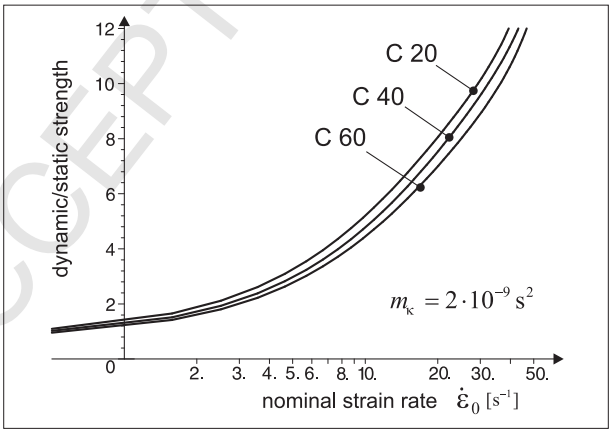

Fig. 14. Tensile strength all concrete grades depending on nominal strain rate

strength increase, which is related to the quasistatic tensile strength, varying with the nominal strain rate for all investigated concrete grades. Principally the same

behavior is given for all concrete grades, where lower grades have a slightly higher relative strength increase compared to higher grades with the same damage inertia.

Uniaxial tensile wave propagation with continuously increasing strains has been investigated in this study, whereas the influences of kinematic boundary conditions and reflections are not considered. Thus, a very special but basic case has been discussed, which has been chosen to point out the principal behavior of a model with inertially retarded damage. Other uniaxial cases can be investigated with the same method. Loading histories with high peak values but limited duration might be of particular interest, furthermore stress waves reflected at free and fixed boundaries. All these investigations exceed the scope of this paper and have to be discussed in further work. As the proposed formulation basing on Eqns. (1,15,21) can immediately be used for plane stress, plane strain, axially symmetric or fully triaxial situations, a plane problem is additionally examined in the following.

7 Application for a plane stress problem

A simple beam under impact loading is numerically investigated in the following. The geometry, boundary conditions and loading are shown in Fig. 15. Plane stress conditions are assumed. The load shape is given with a half-sine, whereby the duration is fixed with $10^{-4}\,\mathrm{s}$ and the magnitude P is variable. A concrete grade C 40 is chosen for this problem with an initial modulus of elasticity $E = 36\,000\,\mathrm{MN/m^2}$ and a specific mass $\varrho = 2.4 \cdot 10^{-3}\,\mathrm{MN\,s^2/m^4}$. The largest natural period according to the beam theory is $T = 0.0147\,\mathrm{s}$. With a tensile strength of $f_{ct} = 3.5\,\mathrm{MN/m^2}$ the static load capacity amounts to $P_{stat} = 0.094\,\mathrm{MN}$. The system's symmetry is utilized for the discretization, whereby 1074 nodes and 1000 four-node quadrilaterals are chosen. The implicit Newmark β-method is again used for time integration. The

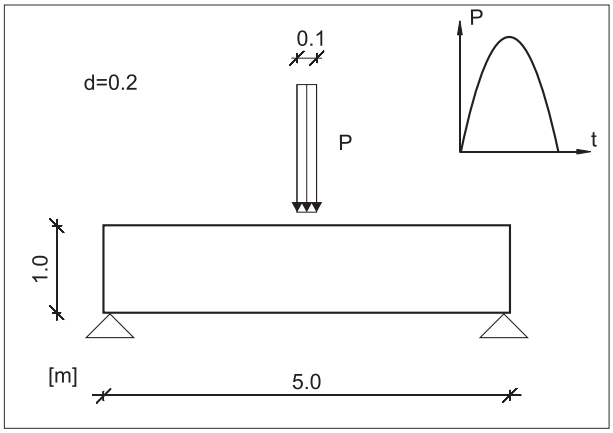

Fig. 15. Impact beam system

very short load duration allows load magnitudes far beyond the static load capacity due to inertial effects. Thus, the immediate area of load contact at the central upper beam edge plays a central role. System failure occurs as a local failure with a total destruction of this area, i.e. a damage parameter $D = 1$. Global failure, i.e. beam bending with an overall utilization of cross-sections, is not relevant in this case.

As a first case a damage inertia $m_\kappa = 2 \cdot 10^{-9}\,\mathrm{s}^2$ is assumed, see Fig. 13. In a computation series the dynamic load carrying capacity, i.e. the maximum magnitude of the short time load without failure, is determined with $P = 5.70\,\mathrm{MN}$. Corresponding vertical displacement-time curves are given in Fig. 16, where A marks the central node at the top side, and B marks the central node at the bottom side. As long as the loading acts on the beam, a vertical compression takes place, with lateral tensile strain rates in the magnitude of $20\,\mathrm{s}^{-1}$. The loading stage is followed by a beam type oscillation with nearly the same displacements of corresponding top and bottom nodes. A displacement reversal occurs at a time $t = 0.0038\,\mathrm{s}$, which corresponds to a quarter of the largest natural period. Computation is stopped at $t = 0.005\,\mathrm{s}$, but system oscillation goes on infinitely. Maximum damage values occuring in the impact area within the dynamic load duration are plotted in Fig. 17 for the above-mentioned computation series with varying load magnitudes. Dam-

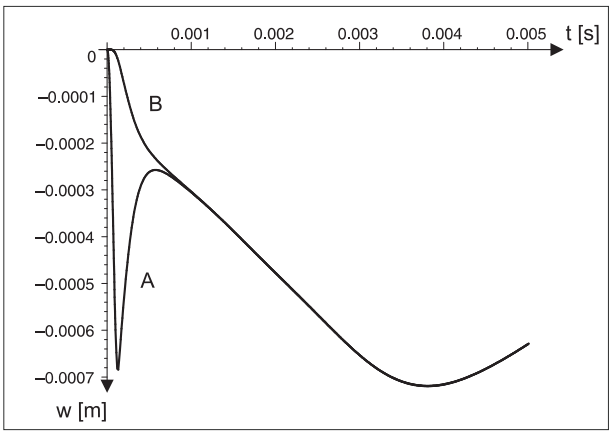

Fig. 16. Impact beam vertical displacements

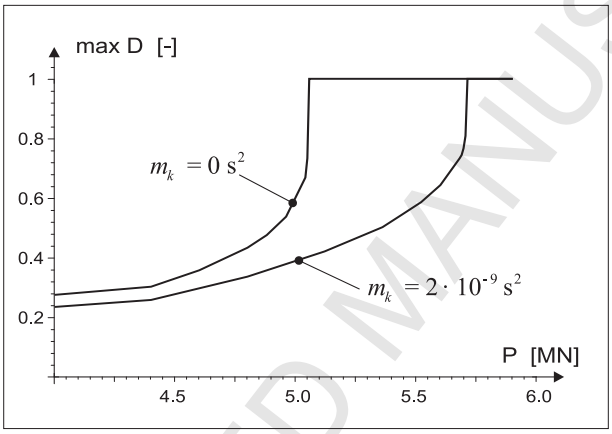

Fig. 17. Max. damage in the impact area during dynamic load duration

age values at the end of the load duration will not grow during the free oscillation.

To determine the influcence of the damage inertia an alternative computation series is performed with a value $m_\kappa = 0$. A system failure as described above occurs with dynamic load magnitude of $P = 5.05\,\mathrm{MN}$. Again the maximum damage values within the load duration are given in Fig. 17 depending on the varying load magnitudes of the computation series. The computed load increase due to damage inertia is $0.65\,\mathrm{MN}$ in this particular case, which makes 7 times the static load carrying capacity. This roughly corresponds to the tensile strength increase factor of Fig. 13 with a strain rate in the magnitude of $20\,\mathrm{s}^{-1}$. It should be clear, that these rough estimations need further elaboration and validation, but this exceeds the scope of

this paper. Another aspect concerns a comparison with experimental results. This is a problem in high speed dynamics of structural members. No testing facilities are available to generate predefined load shapes in the magnitude of meganewtons within fractions of milliseconds, as it is necessary to extract the strain rate effect.

8 Summary and Conclusions

The continuum based damage approach generally has proven to be suitable for the description of concrete behavior. A major characteristic of this approach is given with softening, which is connected with localization phenomena. Thus, continuum models have to be regularized, which can be done with gradient continuum damage. This introduces nonlocal damage as a further variable beneath displacements or strains, respectively. The relation between nonlocal damage and strains is ruled by a differential regularization equation. Its usual form can be extended with an inertial term, which inserts acceleration and inertia of nonlocal damage. Damage inertia in a first approach is assumed as a material constant. The extended regularization equation can be incorporated in finite element methods and solved with standard methods. The application is demonstrated with uniaxial tensile stress wave propagation, where the applied loading corresponds to constant strain rates. The maximum values of the computed stresses by far exceed the quasistatic strength, depending on the nominal strain rate and the assumed value of damage inertia. As constant strain rate conditions lead to continuously increasing strains, the dynamic stress increase beyond the quasistatic strength has only a limited duration and is not a sustainable effect for this particular type of loading. Moreover a beam under impact loading has been investigated as an example for a plane stress problem. Compared to the case without retarded damage an increase of the load leading to

the destruction of the impact area has been computed when damage inertia was active.

A further field remains with the experimental validation, where uniaxial Split-Hopkinson-Bar experiments seem to be most reliable. Nevertheless, special considerations have to be untertaken for concrete specimen, in particular questions remain with the specimen size. It has to be as small as possible to avoid dispersion effects due to lateral deformations and to have a homogenous deformation state. But this is limited by the heterogeneity of concrete, which requires at least 2-3 times the largest aggregate size as specimen diameter. The size restriction could be released, if experimental results are combined with computational simulations. Thus, the influence of a variable specimen length and diameter on the experimental results can also be used to validate the simulation model, as the two-dimensional numerical model allows to consider dispersion effects and nonhomogenous states. A first validation point concerns the question, whether a simple concept with damage inertia as a material constant holds or has to be extended. Furthermore, combinations of intertially retarded damage with e.g. viscoelasticity and viscoplasticity have to be regarded to cover a broader range of strain rates.

References

[1] P. Bischoff, S. Perry. Compressive behavior of concrete at high strain rates. Materials and Structures 24 (1991) 425–450.

[2] L. J. Malvar, C. A. Ross. Review of strain rate effects for concrete in tension. ACI Materials Journal 95 (1998) 735–739.

[3] Y. Lu, K. Xu. Modelling of dynamic behaviour of concrete materials under blast loading. International Journal of Solids and Structures 41 (2004) 131–143.

[4] X. Q. Zhou, H. Hao. Modelling of compressive behaviour of concrete-like materials at high strain rate. International Journal of Solids and Structures 45 (2008) 4628–4661.

[5] H. Kolsky. An investigation of the mechanical properties of materials at very high rates of loading. Proc. Physical Society, Section B 62 (1949) 676–700.

[6] S. Hiermaier. Structures Under Crash and Impact. Springer Verlag, New York, 2008.

[7] A. J. Zielinski. Fracture of concrete and mortar under uniaxial impact tensile loading. Ph.D. thesis, Delft University of Technology (1982).

[8] C. A. Ross, T. Y. Thompson, J. W. Tedesco. Split-Hopkinson-pressure-bar tests on concrete in tension and compression. ACI Materials Journal 86 (1989) 475–481.

[9] S. Zheng, J. Eibl, U. Häußler-Combe. New approach to strain rate sensitivity of concrete in compression. Journal of Engineering Mechanics 125 (1999) 1403–1411.

[10] H. Wu, Q. Zhang, F. Huang, Q. Jin. Experimental and numerical investigation on the dynamic tensile strength of concrete. International Journal of Impact Engineering 32 (2005) 605–617.

[11] A. Brara, J. R. Klepaczko. Experimental characterization of concrete in dynamic tension. Mechanics of Materials 38 (2006) 253–267.

[12] H. Schuler, C. Mayrhofer, K. Thoma. Spall experiments for the measurement of the tensile strength and fracture energy of concrete at high strain rates. International Journal of Impact Engineering 32 (2006) 1635–1650.

[13] P. Forquin, G. Gary, F. Gatuingt. A testing technique for concrete under confinement at high rates of strain. International Journal of Impact Engineering 35 (2008) 425–446.

[14] CEB-FIP (Ed.), Model Code 1990. Thomas Telford, London, 1993.

[15] A. K. Pandey, R. Kumar, D. K. Paul, D. N. Trikha. Strain rate model for dynamic analysis of reinforced concrete structures. Journal of Structural Engineering 132 (2006) 1393–1401.

[16] F. Barpi. Impact behaviour of concrete: a computational approach. Engineering Fracture Mechanics 71 (2004) 2197–2213.

[17] J. Georgin, J. Reynouard. Modeling of structures subjected to impact: concrete behaviour under high strain rate. Cement & Concrete Composites 25 (2003) 131–143.

[18] A. Suffis, T. A. A. Lubrecht, A. Combescure. Damage model with delay effect: Analytical and numerical studies of the evolution of the characteristic damage length. International Journal of Solids and Structures 40 (2003) 3463–3476.

[19] J. Eibl, B. Schmidt-Hurtienne. Strain-rate-sensitive constitutive law for concrete. Journal of Engineering Mechanics 125 (1999) 1411–1420.

[20] L. J. Sluys. Wave propagation, localization and dispersion in softening solids. Ph.D. thesis, Delft University of Technology (1992).

[21] J. Lemaitre, R. Desmorat. Engineering Damage Mechanics. Springer Verlag, Berlin, 2005.

[22] S. Hsieh, E. Ting, W. Chen. A plasticity fracture-model for concrete. International Journal of Solids and Structures 18 (1982) 181–197.

[23] U. Häußler-Combe, J. Hartig. Formulation and numerical implementation of a constitutive law for concrete with strain-based damage and plasticity. International Journal of Non-Linear Mechanics 43 (2008) 399–415.

[24] Z. Bazant, M. Jirasek. Nonlocal integral formulations of plasticity and damage: survey of progress. Journal of Engineering Mechanics 128 (2002) 1119–1149.

[25] M. Jirasek. Nonlocal models for damage and fracture: comparison of approaches. International Journal of Solids and Structures 35 (1998) 4133–4155.

[26] R. Peerlings, R. de Borst, W. Brekelmans, J. de Vree. Gradient enhanced damage for quasi-brittle materials. Int. J. Numer. Meth. Engng. 39 (1996) 3391–3403.

[27] J. Pamin. Gradient-enhanced continuum models: formulation, discretization and applications. Vol. Monograph 301, Cracow University of Technology, Cracow, Poland, 2004.

[28] L. J. Sluys, R. de Borst. Rate-dependent modelling of concrete fracture. Heron 36 (1991) 3–15.

548 **List of Tables**

concrete grade	C20	C40	C60
Young's modulus E $[\mathrm{MN/m^2}]$	30 000	36 000	41 000
Poisson's ratio ν	0.20	0.20	0.20
compressive strength f_c $[\mathrm{MN/m^2}]$	25	50	70
strain ϵ_c at compressive strength	$-2.2 \cdot 10^{-3}$	$-2.5 \cdot 10^{-3}$	$-2.7 \cdot 10^{-3}$
tensile strength f_{ct} $[\mathrm{MN/m^2}]$	2.2	3.5	4.6
crack energy G_f $[\mathrm{Nm/m^2}]$	50	70	95
damage exponent g_d	2.0	2.0	2.0
damage parameter e_0	$-1.54 \cdot 10^{-3}$	$-6.77 \cdot 10^{-6}$	$6.58 \cdot 10^{-4}$
damage parameter e_d	$3.79 \cdot 10^{-3}$	$3.25 \cdot 10^{-3}$	$2.98 \cdot 10^{-3}$
parameter a_1	2.2587	3.1819	3.4522
parameter a_2	0.5334	-0.3419	-0.6140
parameter a_3	8.7041	11.7710	12.6965
parameter a_4	3.6576	4.4077	4.6183

Table 1

Material parameters (concrete grades see [14])